2020-03

Using spatial patterns of fluvial incision to constrain continental-scale uplift in the Andes

Evenstar, LA

10.1016/j.gloplacha.2020.103119
Global and Planetary Change
Elsevier BV

Using spatial patterns of fluvial incision to constrain continental-scale uplift in the Andes.

L.A. Evenstar*[1], A.E. Mather[2] and A.J. Hartley[3]

[1]School of Environment and Technology, University of Brighton, UK,
[2]Department of Geography, Earth and Environmental Sciences, University of Plymouth, UK,
[3]Department of Geology and Petroleum Geology, University of Aberdeen, Aberdeen, UK,

Abstract

Geomorphic archives, particularly longitudinal river profiles, are increasingly used as a proxy to reconstruct uplift rates in mountainous regions. Within the Atacama Desert, Northern Chile, slow, long-term erosion creates exceptional preservation of fluvial and alluvial surfaces. This enables river incision patterns to be used on a continental-scale (>250 km) along the western margin of the Andes (18°00'S to 20°15'S) and over a time frame from Miocene to Present day. The data show marked compartmentalisation of fluvial system behaviour with changes in incision rates from south to north creating 3 distinctly different regions. Within these different sectors, incision rates are broadly consistent between rivers suggesting a regional rather than a river specific control on rates. In Sector 1 (18°05'S to 19°20'S) the fluvial systems are exorheic with a terminal base level (the lowest base level to which the river system can erode) in the Pacific Ocean and span the Coastal Cordillera, Longitudinal Valley, Precordillera and western edge of the Western Cordillera. This constrains the total uplift over these regions to a minimum of 1200 m in 11 Myr with incision rates of ~200-120 m/Myr consistent with rapid but sustained uplift of the Andes in the Late Miocene. In Sector 2 (19°20'S to 19°50'S), to the immediate south, the rivers are shorter and terminate in the Longitudinal Valley, spanning only the Longitudinal Valley, Precordillera and the western edge of the Western Cordillera with lower incision rates of 100-50 m/Myr. Comparison of incision rates between Sector 1 and 2 can constrain the uplift of the Coastal Cordillera to 60m/Myr which is in keeping with previous studies from the region. In southernmost Sector 3 (19°50'S to 20°10'S), the fluvial systems terminate in the Longitudinal Valley and span only the Longitudinal Valley and eastern part of the Precordillera with low incision rates of 50 to 25 m/Myr.

Differences between Sectors 2 and 3 are attributable to drainage loss by tectonic beheading of catchments through uplift of the Cordillera de Domeyko fault system, placing a minimum constrain on uplift in this region of 50 to 25 m/Myr. This study demonstrates the applicability of large-scale fluvial archives to access not just the timing of uplift on a continental scale, but also the relative uplift of individual tectonic provinces.

Keywords; Andes; Paleosurface; Atacama; Desert Pavement; landscape evolution; climate; base levels; fluvial incision, fluvial archives, terraces.

1. Introduction

Fluvial geomorphological archives are being increasingly used to reconstruct climate and deformation (e.g. Macklin et al., 2002, Bridgeland et al., 2012, Stokes et al. 2017, Evenstar et al. 2018; Stokes et al., 2018). These archives comprise dominantly erosional (e.g strath terrace) through to depositional records (e.g. distributive fluvial systems) and can be regionally extensive (e.g. pediment systems). The common theme is that these types of geomorphic archive have low angle surface expressions which can be reconstructed to enable surface deformation to be quantified (e.g. Gesch et al., 2014; Demoulin et al 2017, Stokes et al., 2018). Typically the majority of these studies concentrate on a single pediment surface over small basin scale or focus on trunk drainage or tributaries along a single river system (e.g. Anton et al., 2014, Martins et al., 2017, Evenstar et al., 2018). Whilst correlation of fluvial system behaviour has been attempted across regional scales (>100's km) to examine climate controls (e.g. Macklin et al, 2002), flooding records (e.g. Benito et al., 2000) and uplift rates (Litchfield and Berryman 2006) this has typically been restricted to time-scales younger than the Pliocene. The few studies that look at regional scale deformation over longer timescales tend to utilise modelling of profiles or terrace patterns due to limited preservation of the fluvial system (e.g. Demoulin et al., 2007, Boulton et al., 2014). Where appropriate records are well preserved (e.g. in arid landscapes), availability of high-resolution satellite data sets facilitate regional geomorphic reconstruction over much wider spatial and temporal scales than was previously possible.

The Atacama is the most arid and potentially, oldest desert region in the world (Hartley et al., 2005, Dunai et al., 2005). The long term sustained arid climate leads to preservation of ancient landscapes, some of which are dated back to the Late

Oligocene (Dunai et al. 2005, Evenstar et al. 2009, Evenstar et al. 2017). Several of these surfaces are identified as being generated following abandonment of fluvial incision events associated with fluctuating climate and long-term uplift of the Andean mountain chain (Evenstar at al. 2017). Within hyper-arid fluvial systems, as a function of their low geomorphic erosional efficiency, even modest vertical crustal uplift is likely to be more directly expressed as surface uplift, and thus more likely to be recorded within fluvial archives (e.g. Demoulin et al., 2017). In the central Andes (Atacama Desert) the sustained dominance of extreme aridity is expressed by the presence of near linear to convex hypsometric curves that are typical of areas experiencing ineffective fluvial incision (Montgomery et al., 2002). This incision, in response to tectonic uplift, is documented in the fluvial archives, and along with the past climate (e.g. Dunai et al., 2005; Evenstar et al., 2009; Evenstar et al., 2017), these fluvial archives are increasingly well understood (Victor et al., 2004, Farías et al., 2005, Jordan et al., 2014, van Zalinge et al., 2017) and can be exploited to examine continental scale uplift. These approaches have documented vastly different rates of fluvial incision in northern Chile from 100 m/m.y. (Hoke et al., 2007) to 10 m/m.y (Cooper et al., 2016) since the Middle Miocene leading to different models for timing of Andean uplift.

Here, we utilise freely available satellite remotely sensed data, together with longer term geological and geomorphological erosional and depositional records to reconstruct and quantify the last 11 Myr of pediment and fluvial landscape erosion along the western side of the Central Andes orogen, a classic subduction zone setting. The low erosional efficiency of this landscape means that the surface uplift is preserved in excellent detail. The present study seeks to establish a continental scale view of the fluvial incision and how this varies parallel to the Andean Mountain chain. Using this we aim to establish the main controlling factors on incision rates in order to better understand their use in constraining continental scale uplift within the Central Andes.

2. Study area: landscape components and depositional record

The study region runs along the western margin of the Central Andean mountain range from 18°00’S to 20°15’S (Figure 1a). This region consists of several different morphotectonic provinces; the Coastal Cordillera, Longitudinal Valley, Precordillera and Western Cordillera (Figure 1a). The Coastal Cordillera runs along the coast of the Pacific Ocean and is characterised by the eroded Jurassic magmatic arc. The Coastal Cordillera is absent around the border between Chile and Peru (18°30’S) but

increases in width and height towards the south (Madella et al., 2017). The Coastal Cordillera shows exhumation back to the Eocene (Juez-Larre et al., 2010). However the timing of uplift of this range is poorly constrained with rates varying from 0.001mm/yr to 0.1 mm/yr proximal to the coast (Regard et al. 2010; Garcia-Perez et al., 2018) to 0.05 mm/yr to 0.07 mm/yr inland (Hartley et al., 2000; Dunai et al., 2005; Cosentino and Jordan 2017). On the regional scale the mountain range was still at or close to sea level in the Late Oligocene forming the regionally extensive Tarapaca surface that graded down to sea level (Noble et al., 1985, Delouis et al., 1998, Dunai et al., 2005; Thouret et al., 2007). The mountain range is believed to have uplifted continuously from the late Oligocene at an average rate of 0.05 mm/yr to 0.07 mm/yr (Delouis et al., 1998; Hartley et al., 2000; Dunai et al., 2005; Cosentino and Jordan 2017). To the east, the Coastal Cordillera borders the Longitudinal Valley, a deep fore arc basin infilled with Oligocene to Miocene aged sediments derived from the Andean mountain range to the east (Evenstar et al., 2009; Hartley & Evenstar 2010). The top of the basin is characterized by an elevated low-relief relict landscape termed the Pacific Paleosurface (PPS) (Evenstar et al., 2017). The Longitudinal Valley is characterized by a series of westward propagating reverse faults or monocline folds which have been active from ~30 to 5 Ma (Victor et al., 2004, Garcia 2005, Farías et al., 2004). To the east of the Longitudinal Valley lies the Precordillera. This rises in elevation from 2000 to 4000 masl and is characterized by a series of westward propagating, north-south striking thrusts and folds related to the Domeyko fault system (Figure 1). The Precordillera forms the foothills to the modern magmatic arc in the east, termed the Western Cordillera with peaks up to 6000 m.

The Precordillera and Longitudinal Valley are infilled by volcaniclastic and fluvial sediments, which were predominantly deposited syn-tectonially (Figure 2). The oldest sediments in the region are the Azapa Formation, a series of alluvial conglomerates dated at ~35 to 22.7 Ma (Wörner et al., 2000; Wotzlaw et al., 2011; van Zalinge et., 2017). Overlying the Azapa Formation in the Longitudinal Valley, and unconformably overlying the basement in the Precordillera, are a series of ignimbrites and volcaniclastic sediments termed the Oxaya Formation (22.7 Ma -19.7 Ma) (Wörner et al., 2000; van Zalinge et., 2017). North of 19°00'S, these deposits are predominantly formed by thick ignimbrite sheets (up to 1000 m) (van Zalinge et al., 2017). In the area around the Lluta Quebrada, the ignimbrite sequence forms the top of the stratigraphic succession in the Longitudinal Valley (Figure 2 and 3). In contrast, towards the south, the ignimbrite sheets thin and are intercalated with more fluvial sediments (Hartley and Evenstar, 2010). South of Quebrada Lluta, the volcaniclastic

sediments in the Longitudinal Valley are conformably overlain by the El Diablo Formation (Figure 2), a series of fluvial sediments dated at 16 -11 Ma (Evenstar et al., 2017). Within this region the El Diablo Formation is overlain by the Tana lava dated at 8.8 ± 0.5 Ma (Mortimer et al., 1974) and 8.2 ± 0.5 Ma (Muñoz and Sepulveda, 1992) constraining the age of the end of the El Diablo Formation to 11-8 Ma.

This study focuses on the PPS which is formed from numerous distributive fluvial systems, which can be found in the Longitudinal Valley and in parts of the Precordillera (Evenstar et al., 2017). North of 19°20'S, the PPS is deeply dissected (up to 1,700 masl) by five main rivers (Lluta, Azapa, Victor, Camarones and Tana) that drain to the Pacific Ocean (exorheicly drained) with a terminal base level of 0 masl (Fig. 1). Analysis of the fluvial profiles of Quebrada Tana shows that the main knickpoint is within the Coastal Cordillera (Garcia et al., 2011; Evenstar et al., 2017; Kirk-Lawlor et al., 2013), suggesting that it has not yet adapted to the new terminal (0 masl) base level, with the upper reaches of the river still grading down to the former terminal base level within the Longitudinal Valley at 1000 masl (Kirk-Lawlor et al., 2013; Evenstar et al., 2017). The timing of when fluvial regions north of Quebrada Tana became exorheicly drained is considered to be diachronous from the Early to Mid Miocene (Evenstar et al., 2017). South of this region, the main rivers (Aroma, Tarapaca, de Parca and Tambillo) terminate within the Longitudinal Valley (endorheicly drained) with terminal base levels of ~1000 masl and incise the PPS towards the Western Cordillera by up to 1000 masl (Hoke et al., 2007).

The PPS can be traced for over 600 km (south to north) within the Longitudinal Valley. The surface has been mapped in detail using remote sensing techniques and constrained in age using cosmogenic isotope dating techniques in Evenstar et al., (2017). This research demonstrates that the PPS is in fact formed from an amalgamation of geomorphic surfaces (both erosional (inset) and depositional (overlying)) spanning a range of ages from the Late Oligocene to present day (Evenstar et al., 2009; 2017). The timing of formation of the surface is related to regional climate while the geographical location of the individual components that comprise the surface are controlled by regional tectonic activity (Evenstar et al., 2017). Within the present study we examine the youngest three geomorphic surfaces; Aggradational Surface 4 (AS4), Degradational Surface 3 (DS3) and Degradational Surface 2 (DS2) (Terminology after Evenstar et al., 2017 and shown in Figure 2 and 3). Aggradational surface 4 (AS4) represents the end of deposition of

the El Diablo formation and is dated at 11 Ma using *insitu* exposure ages (Evenstar et al., 2017). Degradational surface 3 (DS3) is an erosion system which cuts into the underlying sediment fill of the basin (El Diablo Formation and Oxaya Formation). The surface comprises a relict dendritic drainage pattern abandoned at ~7 Ma (*insitu* exposure ages, Evenstar et al., 2017). Degradational System 2 (DS2) cuts into the older geomorphic surface DS3 and is characterized by a trellis drainage pattern. The abandonment of this surface is constrained at ~3 Ma (Evenstar et al., 2017). Along the Quebrada Lluta, lies a large (26 km^3) landslip deposit, the Lluta collapse, which disrupts various surfaces. This feature shows westward collapse into the Longitudinal Valley and is believed to have formed at ~3 Ma (Wörner et al., 2002: Kober et al., 2007; Evenstar et al., 2017).

The timing and rate of uplift of the Andes is still ambiguous, with two favoured end-member models (Fig. 2); (1) rapid, late Miocene uplift, with surface uplift of ~2.5 km between 11 and 6 Ma (e.g. Garzione et al., 2006; Ghosh et al., 2006, Garzione et al., 2008); and (2) slow and steady uplift that started in the late Eocene (e.g. Victor et al., 2004; Hartley et al., 2007; Barnes and Ehlers, 2009; Evenstar et al., 2015; van Zalinge et al., 2017). Thus, the eastern edge of the PSS has experienced substantial cumulative surface uplift regardless of which model is taken throughout the Miocene and Pliocene. Several studies have used the main fluvial systems in the region to calculate regional uplift of the Andes across the region (e.g. Farías et al., 2005, Hoke et al., 2007; Schildgen et al., 2002; Schildgen et al., 2009). However, more recent climate modelling of this region has cast doubt on this interpretation suggesting higher incision rates could be due to increased orographically generated precipitation (Ehlers and Poulsen, 2009).

Along the western margin of the Andes, the PPS has been undergoing uplift since at least the Early Miocene (Evenstar et al., 2015) and likely extends back further to the early Oligocene (Barnes and Ehler 2009, van Zalinge et al., 2017). The uplift of the region is modified locally predominantly north-south fault systems (Figure 1) (Wörner et al. 2002; Victor et al. 2005; Farías et al. 2005; van Zalinge et al. 2017) with minor amounts of surface uplift expressed as regional tilting (Farías et al. 2005). However, there are no marked changes in regional tectonic uplift from North to South over the study area with similar rates and timing of uplift (2500m to 3200m of uplift during 25 Ma to 8 Ma) reported from 18°S to 22°S in Northernmost Chile by numerous authors (Wörner et al., 2002; Victor et al., 2005; Farías et al., 2005; Jordan et al., 2014; Evenstar et al., 2015; van Zalinge et al., 2017).

3. Study area climate

The past climate of the region is reasonably well constrained (Fig. 2). The climate has been arid to semi-arid since at least the late Jurassic (Hartley et al., 2005), arid since the late Oligocene and predominantly hyperarid since the mid Miocene (Evenstar et al., 2009, Jordan et al., 2014, Evenstar et al., 2017, Rech et al., 2019). Since the Oligocene, short intervals (< 1 myr) of slightly more humid conditions have been recorded (Evenstar et al., 2009, 2015, 2017; Jordan et al., 2014) (Fig. 2). These humid intervals are within the range of an arid climate with annual mean precipitation rates less than 100 mm/yr, below the threshold for the establishment of significant vegetation cover (Jordan et al., 2014). As a result of the long-lived regional persistent climatic aridity, the PPS is exceptionally well preserved, providing a unique opportunity to examine the development of regionally extensive paleo-fluvial surfaces in a non-vegetated regime over geologic time-scales.

4. Methodology and Approach

4.1 Reconstructing regional fluvial palaeo-surfaces.

Relict paleo-surfaces of the PPS combined with the elevation data in the Longitudinal Valley were used to identify and extrapolate geomorphic surfaces (pediments and valley bottoms) throughout the past ca. 11 Myr. Four regional elevation profiles (A-D) were constructed across the PPS, one parallel to the drainage (A-East to West) and three perpendicular to the drainage (B, C and D-North to south) (Fig. 3). The landscape profiles were constructed using DEM data from Shuttle Radar Topography Mission (SRTM) data with 30 m resolution (Figs. 3 and 4). Profile A is 45 km long and runs from east to west at 18°45'S (Fig. 3). The three other topographic profiles are 260 km long and run parallel along the eastern edge of the Longitudinal Valley from southern Peru at 18°05'S towards northern Chile at 20°15'S (Location in Figure 3 and cross sections in Figure 4). These profiles cross three of the main paleo-surfaces mapped within the regions (AS4, DS3 and DS2) (Fig. 3). On each profile the remnant parts of the various paleo-surfaces (as mapped by Evenstar et al, 2017) are highlighted (Figs.3 and 4). Using the preserved remnants of these surfaces (palaeosurface residual highs, inset terraces and valley bottom elevations) we can extrapolate the line of maximum incision levels of the main quebradas across the region (Figs.3 and 4).

Surface AS4 is formed as a series of relict distributive fluvial systems with a low gradient slope and is preserved on the west edge of profile A forming a plateau (Fig. 3). Using the slope of AS4, the surface can be projected towards the east (Fig. 3). Within profiles B-D, AS4 is preserved in the south as a series of relict inselberg surfaces which can be correlated across the southern region to reconstruct the paleo fluvial surface (Fig. 4). Towards the north of Quebrada Camarones, the preservation of the AS4 surface decreases and the surface cannot be accurately mapped north of Quebrada Lluta.

Surface DS3 formed as a tributive fluvial system incised into AS4. It is well preserved within the central parts of profile A cutting into AS4 and forming a low angle erosional surface. This surface can be projected to the east using the slope angle (Fig. 3). Within profiles B-D, DS3 is mapped as a series of relict inselberg highs north of Quebrada Lluta (Figs. 4 and 5A-B). These highs in profiles B-D can be linked across the region forming a single surface down to Quebrada Camarones. South of this point, where AS4 is preserved, DS3 incises into AS4 and forms a series of lower terraces (Figs. 4 and 5C).

Surface DS2 is preserved along the eastern edge of Profile A cutting into DS3 and forming a low angle erosional surface (Fig. 3). Within Profiles B to D, this surface forms the lowest incision surface north of Quebrada Lluta that can be correlated across this region (Figs. 4 and 5A-B). Towards the south, this surface is constrained within the main quebradas and forms a series of terraces. The Lluta ignimbrite is preserved along these terraces and has previously been used to reconstruct the relict river profiles at 2.7 Ma along the Quebrada Lluta which can be linked with this surface (Kober et al. 2006).

In the southernmost part of the region the laterally traced fluvial archives are correlated with the depths and timing of water table drops in the Cerro Colorado mine that have been reconstructed using hematite age-dates from drill core (Cooper et al. 2016) (Fig. 4). Throughout the region, the present-day fluvial cross-profiles were reconstructed utilising the lowermost incisional points within the modern-day perennial rivers (Fig. 4).

4.2 Palaeo-surface age constraints.

296 Age constraints on the surfaces are based on previously published *insitu* exposure
297 age dating (Kober et al., 2007, Evenstar et al., 2009, Evenstar et al., 2017), dated
298 volcanics (Wörner et al., 2002, Kober et al., 2006, Hoke et al., 2007) and hematite
299 age-dates from drill core (Cooper et al., 2016). These constraints are shown where
300 they intersect the elevation profiles in Figure 4.
301
302 Surface AS4 is constrained as having formed between ~16-8 Ma (Hoke et al., 2007,
303 Evenstar et al., 2015). Within Quebrada Aroma (Fig. 1), the Nama ignimbrite is
304 interbedded with sediments that underlie surface AS4 placing an upper age
305 constraint of 16.27 ± 0.16 Ma on this surface (Pinto et al., 2004, Victor et al., 2004;
306 Farías et al., 2005; Pinto et al., 2007). Proximal to Quebrada Tana (Figs.1 and 4), the
307 Tana lava overlying this surface is dated at 8.8 ± 0.5 Ma (Mortimer et al., 1974 and
308 8.2 ± 0.5 Ma; Muñoz and Sepulveda, 1992) placing an upper age constraint on the
309 surface (Hoke et al., 2007). This surface is further constrained by *insitu* exposure
310 age dating to ~11 Ma (Fig. 4) (Evenstar et al., 2009, Evenstar et al., 2015 and
311 Evenstar et al., 2017).
312
313 Surface DS3 is constrained using *insitu* exposure age dating across the region to ~7
314 Ma (Kober et al., 2006, Evenstar et al., 2009, 2017). Several of the *insitu* exposure
315 ages lie on the landscape cross-profiles either on top of the residual palaeosurfaces
316 in the north or on the incised terrace surfaces in the south and are highlighted in
317 Figures 4 and 5C. Proximal to the Cerro Colorado mine DS3 links with the depth and
318 age of dated hematite within drill core at 7 Ma which records the paleowater table
319 level (Cooper et al., 2016) (Figure 4).
320
321 Surface DS2 was dated at ~3 Ma based on *insitu* exposure age dating (Fig. 4)
322 (Kober et al., 2006, Evenstar et al., 2009, 2017). The surface age can be further
323 constrained using the preservation of the Lluta ignimbrite (dated at 2.7 Ma; Wörner et
324 al., 2002) along fluvial terraces within Quebradas Lluta and Azapa (Fig. 4). Proximal
325 to the Cerro Colorado mine this surface is linked to dated hematite (3 Ma) within drill
326 core (Cooper et al., 2016) (Fig. 4).
327
328 **4.3 Reconstructing regional mean incision rates.**
329
330 The reconstructed fluvial paleo-surface profiles combined with the dating constraints
331 described above can be used to calculate the regional fluvial incision rates over the
332 last 11 million years (Fig. 6A). The difference in elevation between the paleo-fluvial

surfaces and modern river were extrapolated for each surface across the region (Fig. 6B). Using the difference in elevation of the surfaces and the modern river, divided by the time since the surfaces had been abandoned the mean fluvial incision rates along the main quebradas were calculated (Fig. 6C). In this way, we are able to reconstruct relative incision rates for the PSS.

5. Results

Profile A runs 45 km from east to west at 18°45'S in Figure 3 and highlights the general relationship of the surfaces within the region. AS4 is predominantly preserved in the west of the Longitudinal Valley and shows an average depositional slope of 5° to the west. Cutting into AS4 within the centre of the Longitudinal Valley, DS3 incises 90 m and shows a similar depositional slope angle. To the east of DS3, DS2 cuts 90 m into and erodes DS3, with a higher slope angle of 10° to the west. Figure 4 highlights the overall relationship of the main fluvial archives from North to South. AS4 forms the highest elevation surface across the region and is predominantly preserved in the southern parts of the elevation profiles. DS3 cuts into AS4 forming a lower elevation surface across the region. Cutting into both AS4 and DS3, DS2 forms at the lowest elevation of all the preserved paleo-fluvial surface in the Longitudinal Valley. The modern river system forms at the base of the valleys with the lowermost elevations across the region. All the surfaces generally show an increase in elevation towards the east and south across the region (Figure 3 and 4). The changes in elevation show a step like increase from north to south and can be separated into three different sectors (1 to 3 on Figure 4). Sector 1 runs from (18°05'S) to Quebrada Tana (19°20'S), Sector 2 from Quebrada Tana (19°20'S) to Quebrada Tarapaca (19°50'S) and Sector 3 from Quebrada Tarapaca (19°50'S) to Quebrada Juan de Morales (20°10'S). Within each sector the change in elevation is broadly similar and affects a number of different rivers rather than being river specific. Sector 1 shows the highest changes in elevation across the region between the different fluvial surfaces which decrease within Sector 2 and is the lowest within Sector 3.

Figure 6A shows the current elevation of the fluvial systems in cross section B. AS4 shows a single laterally extensive surface which undulates across the region from ~2750 masl in Sector 1, to ~2500 masl in Sector 2 and ~2650 masl in Sector 3. DS3 forms a laterally extensive surface with an average height of 2350 masl across Sector 1 and 2 and increasing in elevation to ~2700 masl in Sector 3. DS2 varies in

370 elevation from 1800 masl at the northern tip of the elevation profile to ~ 2000 masl in
371 Sector 2 and increases in height to ~2600 masl in Sector 3. The modern fluvial
372 systems vary in height from 1400 masl to 1500 masl in Sector 1 to Sector 2 to ~2000
373 masl and ~2500 masl in Sector 3.
374
375 Using the difference between the paleo fluvial surfaces and modern fluvial systems
376 the change in fluvial incision through time can be more clearly illustrated (Fig. 6B).
377 and combined with the age constraint the fluvial incision rates through time can be
378 calculated (Fig. 6C). Overall, fluvial incision shows higher rates from 3 to present
379 day. However, there are marked differences across the study area. Sector 1 show
380 the highest rates of fluvial incision through time from 120 m/Myr at 11-7 Ma to 150
381 m/Myr at 7-3 Ma to ~200 m/Myr at 3-0 Ma. Sector 2 show lower incision rates
382 through time of 50 m/My for both 11-7 Ma and 7-3 Ma and higher rates of 100-50 for
383 3-0 Ma. Sector 3 show the lowest rates of fluvial incision throughout the area with 25
384 m/Myr from 11-7 Ma, 30m/Myr from 7-3 Ma and 50 m/Myr from 3-0 Ma.
385
386 **6. Discussion**
387
388 The geomorphic archive, using both pediplain and fluvial surfaces, is reconstructed
389 from Northernmost Chile and combined with age constraints to calculate fluvial
390 incision rates over a continental scale (>250 km) and back to the Miocene. These
391 data demonstrate three spatially marked changes in incision rates across the region,
392 from north to south. These distinctly different regions have been termed Sectors 1-3.
393 Sector 1 has the highest rates of fluvial incision through time (ca. 200 to 100 m/Myr),
394 Sector 2 show a lower rate of incision (ca. 100 to 50 m/Myr) and Sector 3 has the
395 lowest rates of incision (<50 m/Myr). These profiles show a generally continuous
396 drop in fluvial incision with slightly higher incision from 3 Ma to the present day. This
397 study shows that along the western margin of the Andes rates of fluvial incision can
398 vary dramatically over distances of 10’s to 100’s km. In Sector 1, incision rates of 100
399 m/m.y support those proposed by Hoke et al., (2007). However, in contrast to Hoke
400 et al., (2007) the incision shows a marked decrease to the south of Section 1 with
401 substantially lower rates in Section 2 and Section 3. These low rates correlate with
402 the incision rates documented in Cooper et al., (2016) explaining the disparity
403 between these two studies. Below we discuss what controls the variation in incision
404 rates in this region in order to evaluate their use as surface uplift makers.
405
406 The spatial extent of the area impacted (i.e. affecting multiple rivers per area

simultaneously) implies an external control. Such a control could take the form of (but is not limited to) a change in relative terminal base level, climate or regional scale tectonic uplift through fault blocks, rather than more localised internal river/catchment specific causes (e.g. internal drainage reorganisation via river capture). Below we discuss the major external controls on the compartmentalisation of the rivers within this region.

6.1 Uplift and fluvial incision

Regional tectonic uplift

Fluvial incision rates have been used in numerous studies to help constrain uplift in tectonically active areas (Maddy et al. 1997; Lave and Avouac 2001; Lu et al. 2004; Whittaker et al., 2007). Although fluvial incision rates do not necessarily directly translate to uplift rates as discharge may limit erosional capacity, they do give minimum constraints. The sustained regional uplift of the Andean mountain chain is broadly mirrored by continuous tectonically-driven fluvial incision throughout the Miocene. However, this uplift is predominantly controlled by north-south fault systems creating variation in uplift from West to East. There are no large scale east-west trending structures which would generate marked changes in regional tectonic uplift from North to South accounting for the compartmentalisation of the fluvial incision rates.

Terminal base level

Comparison of Sector 1 and Sector 2 suggests a marked decrease in fluvial incision through time and a marked change in terminal base level between the two fluvial regions. In this part of the Andes the terminal base level is either external (sea level) north of Quebrada Tana or internal (the Longitudinal valley, 1000 masl) south of Quebrada Tana. Uniquely, Quebrada Tana acts as an endorheic drainage within the Longitudinal Valley (Garcia et al., 2011; Kirk-Lawlor et al., 2013; Evenstar et al., 2017). The timing of when fluvial systems north of Quebrada Tana became exorheicly drained is diachronous from the Early to Mid Miocene ***prior*** to the fluvial incision documented here (Evenstar et al., 2017). A change in base level would initially lead to river profile adjustment affecting individual drainages, the absence of observable river specific differences in the fluvial archives support the idea that in Sector 1 rivers had an exorheic drainage prior to 11 Ma and so do not explain the difference in fluvial incision rates between Sector 1 and Sector 2. However, the uplift of the Coastal Cordillera has not been static during this time period. The uplift rate of

444 the Coastal Cordillera is poorly constrained, as discussed above. The base level of
445 the fluvial systems in the Longitudinal Valley terminate onto the eastern edge of the
446 Coastal Cordillera and are therefore affected by the regional scale uplift of the
447 mountain range rather than the uplift proximal to the coast which may be more
448 variable. The large scale and long term uplift of the mountain range varies from
449 between 50 m/Myr (0.05 mm/yr) to 70 m/Myr (0.07 mm/yr) (Delouis et al. 1998;
450 Hartley et al. 2000; Dunai et al. 2005; Cosentino and Jordan 2017). The difference
451 between the fluvial incision rate at Sector 1 compared to Sector 2, averaged over 11
452 Ma is 60m/Myr correlating with this value. Consequently, whilst Andean uplift to the
453 east generated significant fluvial incision within the Longitudinal Valley this was
454 partially offset in Sector 2 and 3 (the endorheicly-drained region) by simultaneous
455 uplift of the Coastal Cordillera in the west. In essence, the rate of fluvial incision is
456 controlled by the east to west length of the fluvial system and whether rivers cut the
457 uplifting north-south trending Coastal Cordillera. The difference between the reach of
458 Sector 1 and Sector 2 is highlighted in Figure 1B.
459
460 **Tectonic beheading**
461
462 The change in fluvial incision rates from Sector 2 to 3 are more challenging to
463 explain. Both sectors have the same terminal base level within the Longitudinal
464 Valley of ~1000 masl. However, there is a sharp change in the catchment length of
465 major fluvial systems entering the Longitudinal Valley from between the two regions
466 (Fig. 7). Throughout the region, 18°20''S to 22°00' S, the fluvial systems have been
467 constrained by Hoke et al., 2007 as ranging in drainage area from 5 x 10^9 km^2 to 9 x
468 10^8 km^2 and in length from 30 to 170 km, with both values decreasing towards the
469 south (Fig. 7). Significantly, these data demonstrate a sudden decrease in fluvial
470 lengths from 110 km to 80 km between Sector 2 and Sector 3 (Figs.1 and 7). This
471 length-gap coincides with a sudden shift in the edge of the watershed from along the
472 western edge of the Western Cordillera to along the Cordillera de Domeyko fault
473 system in the central Precordillera suggesting a tectonically configured watershed.
474 The uplift along the Cordillera de Domeyko fault system beheads the upper part of
475 the drainages within Sector 3, reducing their length by approx. 30 km (Figs. 1 and 7).
476 The affected fluvial systems in this region thus only record the minimum uplift over
477 the Longitudinal Valley and Precordillera as they are no longer connected to the
478 highest elevation areas of the mountain range further east (Fig. 1B). The difference
479 in fluvial incision rates between Sector 2 and Sector 3 of 25 m/Myr to 50 m/Myr
480 therefore place constraints on the uplift generated between the central and eastern

edge of the Precordillera.

6.2 Alternative controls on fluvial incision

Whilst the observed spatial differences in fluvial incision rates over the region can be largely explained by tectonic controls it is important to briefly explore alternative explanations for these regional differences within the study area that can operate on a similar spatial scale, principally climate and bedrock. It has been suggested that the present-day rivers within the study area vary in erosional capacity from north to south as a function of mean annual precipitation within the source regions (Garcia et al 2011). Quebrada Lluta has a catchment with a present-day mean annual precipitation rate of 200 mm/yr, Quebradas Azapa, Victor and Camarones have rates of 100 mm/yr and south of Quebrada Camarones the river catchments have rates of < 100 mm/yr (Garcia et al., 2011). However, it is unlikely that latitudinal variations in rainfall are the main cause for incision patterns observed across the region as there is no apparent spatial link between the precipitation rates and the change in fluvial incision rates. For example, there is no change in the fluvial incision between Quebrada Lluta and the rivers to the south, despite Quebrada Lluta draining an area with much higher mean annual precipitation. If precipitation rates do place some control on incision rates it must be at a much smaller scale than the tectonic controls.

Fluvial research demonstrates that the strength properties of bedrock lithology can impact on fluvial system incisional behaviour (e.g. Stokes et al., 2017) and could thus potentially account for spatial variations in incision rates across the study area. However, whilst there is a difference *between* the major N-S morphotectonic units (thereby presenting an E-W variability in potential erodibility across the region), there is little N-S variation *within* these units that can account for the observed N-S spatially compartmentalised incision rates.

6.3 Controls on fluvial incision in Northern Chile

Fluvial incision rates have been used in numerous studies to help constrain uplift in tectonically active areas (Lave and Avouac 2001; Lu et al. 2004; Whittaker et al., 2007; Anton et al., 2014; Stokes et al. 2018). The fluvial regions along the edge of the Andes have varying east-west extent over the north-south orientated tectonic provinces. The fluvial incision therefore shows marked compartmentalization across the region with a step like increase from south to north. The varying reaches of the

rivers and the differences in fluvial incision rates between these reaches can therefore be exploited to place minimum constraints on the different tectonic provinces through time.

Sector 1, which spans from the Pacific Ocean to the western edge of the Western Cordillera (Figure 1B), constrains the uplift on a continental-scale along the edge of the Andes. This constrains the uplift of this region (the western side of the Andes) to a minimum of 1200m in 11 Myr. This supports previous models of Late Miocene uplift (e.g. Garzione et al., 2006; Ghosh et al., 2006, Garzione et al., 2008) however in contrast to these models it suggests uplift continued at a slower rate from 7 to 3 Ma and at a higher rates from 3 to 0 Ma (120 m/Myr at 11-7 Ma to 150 m/Myr at 7-3 Ma to ~200 m/Myr at 3-0 Ma).

Sector 2 spans from the Longitudinal Valley to the western edge of the Western Cordillera (Fig. 1B) constraining the uplift over the western margin of the Andes minus uplift of the Coastal Cordillera. Therefore, the difference between Sector 1 and Sector 2 of 60 m/Myr records the uplift of the Coastal Cordillera which corresponds with published uplift rates for the Coastal Cordillera of between 50 m/Myr (0.05 mm/yr) to 70 m/Myr (0.07 mm/yr) (Delouis et al. 1998; Hartley et al. 2000; Dunai et al. 2005).

Sector 3, spans a much shorter extent than Sectors 1 and 2, from the Longitudinal Valley to the Cordillera de Domeyko fault system in the central Precordillera (Fig. 1B). The difference between Sectors 2 and 3, of 25 m/Myr to 50 m/Myr, therefore places a minimum constraint on the uplift generated between the central and eastern edge of the Precordillera along the Cordillera de Domeyko fault system.

7. Conclusions

Within the Atacama Desert, Northern Chile, slow long-term erosion creates exceptional preservation of geomorphic archives (fluvial and pediment surfaces) allowing the long-term reconstruction of fluvial archives on a continental scale. In this study, fluvial profiles are constructed over a wide region (>250 km) along the western margin of the Andes (18°00’S to 20°15’S) and over a time frame from Miocene to Present day. The results reveal that incision patterns reconstructed over a wide area running perpendicular to the main fluvial systems allows a greater spatial and temporal understanding of uplift, specifically;

- Fluvial incision can be reconstructed for ~11 Ma, ~7 Ma, ~3 Ma and the modern day.
- Fluvial incision shows marked spatial compartmentalization across the region with a step like increase from south to north.
- Sector 1 has the highest rates of fluvial incision through time (ca. 200 to 100 m/Myr), Sector 2 shows a lower rate of incision (ca. 100 to 50 m/Myr) and Sector 3 has the lowest rates of incision (<50 m/Myr).
- The main control on the rate of fluvial incision is the extent of the east to west reach of the main rivers across the north to south tectonic provinces.
- Sector 1 spans the entire Coastal Cordillera, Longitudinal Valley and Precordillera to the western edge of the Western Cordillera. This constrains uplift of this region (the western side of the Andes) to a minimum of 1200m in 11 Myr which supports Late Miocene uplift however contrary to these models, it suggests uplift continued at a higher rate from 3 to the present day.
- Sector 2 only spans the Longitudinal Valley and the Precordillera to the western edge of the Western Cordillera. The absence of fluvial systems cutting the Coastal Cordillera accounts for the reduced incision rates of 60 m/Myr which correspond to the published uplift rates for the Coastal Cordillera of 60 m/Myr.
- The eastern edge of Sector 3 is constrained by the Cordillera Domeyko fault system within the Central Precordillera. As such, Sector 3 only places constraints on uplift of the Longitudinal Valley and the western edge of the Precorillera. The absence of the eastern edge of the Precordillera accounts for the decrease in incision rates within this area and places a constraint of uplift generated here in the region of 25 m/Myr to 50 m/Myr.

Most Quaternary fluvial studies tend to be restricted to detailed examination of a single river to understand long-term uplift or climate, mainly due to the scale and intensity of research required to unravel the incision history. Whilst this provides a wealth of knowledge regarding uplift over the reach of the fluvial system, in order to understand orographic scale uplift (and rule out river specific controls) a more regional overview of the fluvial base-level changes is required. Such studies have the potential to address not just the timing of uplift on a continental scale but also any regional spatial controls such as the relative uplift of individual tectonic provinces.

8. Acknowledgements

This study was funded by BHP and the University of Brighton Rising Stars. The authors are grateful to Marit Van Zalinge and Masie Mather for discussions on the manuscript.

9. References

Antón, L., De Vicente, G., Muñoz-Martín, A., & Stokes, M. (2014). Using river long profiles and geomorphic indices to evaluate the geomorphological signature of continental scale drainage capture, Duero basin (NW Iberia). Geomorphology, 206, 250-261.

Barnes, J. B., & Ehlers, T. A. (2009). End member models for Andean Plateau uplift. Earth-Science Reviews, 97(1-4), 105-132.

Benito, G., Gutiérrez, F., Pérez-González, A., & Machado, M. J. (2000). Geomorphological and sedimentological features in Quaternary fluvial systems affected by solution-induced subsidence (Ebro Basin, NE-Spain). Geomorphology, 33(3-4), 209-224.

Boulton, S. J., Stokes, M., & Mather, A. E. (2014). Transient fluvial incision as an indicator of active faulting and Plio-Quaternary uplift of the Moroccan High Atlas. Tectonophysics, 633, 16-33.

Bridgland, D. R., Westaway, R., Romieh, M. A., Candy, I., Daoud, M., Demir, T. & Shaw, A. D. (2012). The River Orontes in Syria and Turkey: Downstream variation of fluvial archives in different crustal blocks. Geomorphology, 165, 25-49.

Cooper, F., Adams, B., Blundy, J., Farley, K., McKeon, R., & Ruggiero, A. (2016). Aridity-induced Miocene canyon incision in the Central Andes. Geology, 44(8), 675-678.

Cosentino, N. J., Jordan, T. E., Derry, L. A., & Morgan, J. P. (2015). 87Sr/86Sr in recent accumulations of calcium sulfate on landscapes of hyperarid settings: A bimodal altitudinal dependence for northern C hile (19.5° S–21.5° S). Geochemistry, Geophysics, Geosystems, 16(12), 4311-4328.

Cyr, A. J., Granger, D. E., Olivetti, V., & Molin, P. (2010). Quantifying rock uplift rates using channel steepness and cosmogenic nuclide–determined erosion rates: Examples from northern and southern Italy. Lithosphere, 2(3), 188-198.

Delouis, B., Philip, H., Dorbath, L., & Cisternas, A. (1998). Recent crustal deformation in the Antofagasta region (northern Chile) and the subduction process. Geophysical Journal International, 132(2), 302-338.

Demoulin, A., Bovy, B., Rixhon, G., & Cornet, Y. (2007). An automated method to extract fluvial terraces from digital elevation models: The Vesdre valley, a case study in eastern Belgium. Geomorphology, 91(1-2), 51-64.

Demoulin, A., Mather, A., & Whittaker, A. (2017). Fluvial archives, a valuable record of vertical crustal deformation. Quaternary Science Reviews, 166, 10-37.

Dunai, T. J., Gonzalez-Lopez, G. A., Juez-Larre, J., & Carrizo, D. (2005). Preservation of (early) miocence landscapes in the Atacama Desert, northern Chile. Geochimica Et Cosmochimica Acta, 69(10), A161-A161.

Ehlers, T. A., & Poulsen, C. J. (2009). Influence of Andean uplift on climate and paleoaltimetry estimates. Earth and Planetary Science Letters, 281(3-4), 238-248.

Evenstar, L., Mather, A., Hartley, A., Stuart, F., Sparks, R., & Cooper, F. (2017). Geomorphology on geologic timescales: Evolution of the late Cenozoic Pacific paleosurface in Northern Chile and Southern Peru. Earth-Science Reviews. 71, 1-27.

Evenstar, L. A., Hartley, A. J., Stuart, F. M., Mather, A. E., Rice, C. M., & Chong, G. (2009). Multiphase development of the Atacama Planation Surface recorded by cosmogenic He-3 exposure ages: Implications for uplift and Cenozoic climate change in western South America. Geology, 37(7), 658-658.

Evenstar, L. A., Stuart, F. M., Hartley, A. J., & Tattitch, B. (2015). Slow Cenozoic uplift of the western Andean Cordillera indicated by cosmogenic 3He in alluvial boulders from the Pacific Planation Surface. Geophysical Research Letters, 42(20), 8448-8455.

Evenstar, L. A., Sparks, R. S. J., Cooper, F. J., & Lawton, M. N. (2018). Quaternary landscape evolution of the Helmand Basin, Afghanistan: Insights from staircase terraces, deltas, and paleoshorelines using high-resolution remote sensing analysis. Geomorphology, 311, 37-50.

Farías, M., Charrier, R., Comte, D., Martinod, J., & Hérail, G. (2005). Late Cenozoic deformation and uplift of the western flank of the Altiplano: Evidence from the depositional, tectonic, and geomorphologic evolution and shallow seismic activity (northern Chile at 19°30′S). Tectonics, 24(4), TC4001.

Garcia, M., & Herail, G. (2005). Fault-related folding, drainage network evolution and valley incision during the Neogene in the Andean Precordillera of Northern Chile. Geomorphology, 65(3-4), 279-300.

Garcia, M., Riquelme, R., Farías, M., Herail, G., & Charrier, R. (2011). Late Miocene-Holocene canyon incision in the western Altiplano, northern Chile: tectonic or climatic forcing? Journal of the Geological Society, 168(4), 1047-1060.

García-Pérez, T., Marquardt, C., Yáñez, G., Cembrano, J., Gomila, R., Santibañez, I., & Maringue, J. (2018). Insights on the structural control of a Neogene forearc basin in Northern Chile: A geophysical approach. Tectonophysics, 736, 1-14.

Garzione, C. N., Hoke, G. D., Libarkin, J. C., Withers, S., MacFadden, B., Eiler, J. & Mulch, A. (2008). Rise of the Andes. Science, 320(5881), 1304-1307.

Garzione, C. N., Molnar, P., Libarkin, J. C., & MacFadden, B. J. (2006). Rapid late Miocene rise of the Bolivian Altiplano: Evidence for removal of mantle lithosphere. Earth and Planetary Science Letters, 241(3-4), 543-556.

Gesch, D. B. (2014). An inventory of topographic surface changes; the value of multitemporal elevation data for change analysis and monitoring. ISPRS Annals of Photogrammetry, Remote Sensing & Spatial Information Sciences, 2(4).

Ghosh, P., Garzione, C. N., & Eiler, J. M. (2006). Rapid uplift of the Altiplano revealed through C-13-O-18 bonds in paleosol carbonates. Science, 311(5760), 511-515.

Hartley, A. J., Chong, G., Houston, J., & Mather, A. E. (2005). 150 million years of climatic stability: evidence from the Atacama Desert, northern Chile. Journal of the Geological Society, 162(3), 421-424.

Hartley, A. J., & Evenstar, L. (2010). Cenozoic stratigraphic development in the north Chilean forearc: Implications for basin development and uplift history of the Central Andean margin. Tectonophysics, 495(1-2), 67-77.

Hartley, A. J., May, G., Chong, G., Turner, P., Kape, S. J., & Jolley, E. J. (2000). Development of a continental forearc: A Cenozoic example from the Central Andes, northern Chile. Geology, 28(4), 331-334.

Hartley, A. J., Sempere, T., & Wörner, G. (2007). A comment on "Rapid late Miocene rise of the Bolivian Altiplano: Evidence for removal of mantle lithosphere" by C.N. Garzione et al. [Earth Planet. Sci. Lett. 241 (2006) 543-556]. Earth and Planetary Science Letters, 259(3-4), 625-629.

Hoke, G. D., Isacks, B. L., Jordan, T. E., Blanco, N., Tomlinson, A. J., & Ramezani, J. (2007). Geomorphic evidence for post-10 Ma uplift of the western flank of the central Andes 18°30′-22°S. Tectonics, 26(5), TC5021

Hu, X., Pan, B., Kirby, E., Li, Q., Geng, H., & Chen, J. (2010). Spatial differences in rock uplift rates inferred from channel steepness indices along the northern flank of the Qilian Mountain, northeast Tibetan Plateau. Chinese Science Bulletin, 55(27-28), 3205-3214.

Jordan, T. E., Kirk-Lawlor, N. E., Blanco P., N., Rech, J. A., & Cosentino, N. J. (2014). Landscape modification in response to repeated onset of hyperarid paleoclimate states since 14 Ma, Atacama Desert, Chile. Geological Society of America Bulletin. 126(7/7), 1016-1046

Juez-Larré, J., Kukowski, N., Dunai, T. J., Hartley, A. J., & Andriessen, P. A. (2010). Thermal and exhumation history of the Coastal Cordillera arc of northern Chile revealed by thermochronological dating. Tectonophysics, 495(1), 48-66.

739 Kirk-Lawlor, N. E., Jordan, T. E., Rech, J. A., & Lehmann, S. B. (2013). Late Miocene
740 to Early Pliocene paleohydrology and landscape evolution of Northern Chile, 19 to 20
741 S. Palaeogeography, Palaeoclimatology, Palaeoecology, 387, 76-90.
742
743 Kober, F., Ivy-Ochs, S., Schlunegger, F., Baur, H., Kubik, P. W., & Wieler, R. (2007).
744 Denudation rates and a topography-driven rainfall threshold in northern Chile:
745 Multiple cosmogenic nuclide data and sediment yield budgets. Geomorphology, 83(1-
746 2), 97-120.
747
748 Kober, F., Schlunegger, F., Zeilinger, G., & Schneider, H. (2006). Surface uplift and
749 climate change: The geomorphic evolution of the Western Escarpment of the Andes
750 of northern Chile between the Miocene and present. Tectonics, Climate, and
751 Landscape Evolution, 398, 75-86.
752
753 Lavé, J., & Avouac, J.-P. (2000). Active folding of fluvial terraces across the Siwaliks
754 Hills, Himalayas of central Nepal. Journal of Geophysical Research: Solid Earth,
755 105(B3), 5735-5770.
756
757 Litchfield, N., & Berryman, K. (2006). Relations between postglacial fluvial incision
758 rates and uplift rates in the North Island, New Zealand. Journal of Geophysical
759 Research: Earth Surface, 111(F2).
760
761 Lu, H., Wang, X., An, Z., Miao, X. D., Zhu, R. X., Ma, H. Z., & Wang, X. Y. (2004).
762 Geomorphologic evidence of phased uplift of the north eastern Qinghai-Tibet Plateau
763 since 14 million years ago. Science in the China Series D Earth Science-English
764 edition, *47*, 822-833.
765
766 Macklin, M. G., Fuller, I. C., Lewin, J., Maas, G. S., Passmore, D. G., Rose, J., &
767 Rowan, J. S. (2002). Correlation of fluvial sequences in the Mediterranean basin over
768 the last 200 ka and their relationship to climate change. Quaternary Science
769 Reviews, 21(14-15), 1633-1641
770
771 Maddy, D. (1997). Uplift-driven valley incision and river terrace formation in southern
772 England. Journal of Quaternary Science: Published for the Quaternary Research
773 Association, 12(6), 539-545.
774
775 Madella, A., Delunel, R., Audin, L., & Schlunegger, F. (2016). Why is there no

776 Coastal Cordillera at the Arica Bend (Western Central Andes)? Basin Research.
777 Mortimer C., F. E. a. S. N. (1974). K-Ar ages from tertiary lavas of the northernmost
778 Chilean Andes. Geologische Rundschau, 63, 484 - 493.
779
780 Martins, A. A., Cabral, J., Cunha, P. P., Stokes, M., Borges, J., Caldeira, B., &
781 Martins, A. C. (2017). Tectonic and lithological controls on fluvial landscape
782 development in central-eastern Portugal: Insights from long profile tributary stream
783 analyses. Geomorphology, 276, 144-163.
784
785 Montgomery, D. R., & Brandon, M. T. (2002). Topographic controls on erosion rates
786 in tectonically active mountain ranges. Earth and Planetary Science Letters, *201*(3-
787 4), 481-489.
788
789 Muñoz, N., Sepúlveda, p. (1992). Estructuras compressivas con vergencia al Oeste
790 en el borde oriental de la Depresión Central (19°15' lat. Sur). Revista Geologica De
791 Chile, 19, 214-247.
792
793 Noble, D. C., Sébrier, M., Megard, F., & McKee, E. H. (1985). Demonstration of two
794 pulses of Paleogene deformation in the Andes of Peru. Earth and Planetary Science
795 Letters, 73(2), 345-349.
796
797 Pinto, L., Hérail, G., Charrier, R. (2004). Syntectonic sedimentation associated with
798 Neogene structures in the Precordillera of Moquella Zone, Tarapacá (19°15'S,
799 northern Chile). Revista Geologica De Chile, 31, 19-44.
800
801 Pinto, L., Hérail, G., Fontan, F., & de Parseval, P. (2007). Neogene erosion and uplift
802 of the western edge of the Andean Plateau as determined by detrital heavy mineral
803 analysis. Sedimentary Geology, 195(3-4), 217-237.
804
805 Rech, J. A., Currie, B. S., Jordan, T. E., Riquelme, R., Lehmann, S. B., Kirk-Lawlor,
806 N. E., & Gooley, J. T. (2019). Massive middle Miocene gypsic paleosols in the
807 Atacama Desert and the formation of the Central Andean rain-shadow. Earth and
808 Planetary Science Letters, 506, 184-194.
809
810 Regard, V., Saillard, M., Martinod, J., Audin, L., Carretier, S., Pedoja, K., ... & Hérail,
811 G. (2010). Renewed uplift of the Central Andes Forearc revealed by coastal evolution
812 during the Quaternary. Earth and Planetary Science Letters, 297(1-2), 199-210.

Schildgen, T., Dethier, D. P., Bierman, P., & Caffee, M. (2002). ^{26}Al and ^{10}Be dating of late Pleistocene and Holocene fill terraces: a record of fluvial deposition and incision, Colorado Front Range. Earth Surface Processes and Landforms, 27(7), 773-787.

Schildgen, T. F., Ehlers, T. A., Whipp, D. M., van Soest, M. C., Whipple, K. X., & Hodges, K. V. (2009). Quantifying canyon incision and Andean Plateau surface uplift, southwest Peru: A thermochronometer and numerical modeling approach. Journal of Geophysical Research, 114(F4).

Stokes, M., Mather, A., Belfoul, M., Faik, F., Bouzid, S., Geach, M., & Thiel, C. (2017). Controls on dryland mountain landscape development along the NW Saharan desert margin: Insights from Quaternary river terrace sequences (Dadès River, south-central High Atlas, Morocco). Quaternary Science Reviews, 166, 363-379.

Stokes, M., Mather, A., Rodés, Á., Kearsey, S., & Lewin, S. (2018). Anatomy, age and origin of an intramontane top basin surface (Sorbas Basin, Betic Cordillera, SE Spain). Quaternary, 1(2), 15

Thouret, J.-C., Wörner, G., Gunnell, Y., Singer, B., Zhang, X., & Souriot, T. (2007). Geochronologic and stratigraphic constraints on canyon incision and Miocene uplift of the Central Andes in Peru. Earth and Planetary Science Letters, 263(3), 151-166.

van Zalinge, M. E., Sparks, R. S. J., Evenstar, L. A., Cooper, F. J., Aslin, J., & Condon, D. J. (2017). Using ignimbrites to quantify structural relief growth and understand deformation processes: Implications for the development of the Western Andean Slope, northernmost Chile. Lithosphere, 9(1), 29-45.

Victor, P., Oncken, O., & Glodny, J. (2004). Uplift of the western Altiplano plateau: Evidence from the Precordillera between 20° and 21°S (northern Chile). Tectonics, 23(4), TC4004.

Wörner, G., Hammerschmidt, K., Henjes-Kunst, F., Lezaun, J., & Wilke, H. (2000). Geochronology (40Ar/39Ar, K-Ar and He-exposure ages) of Cenozoic magmatic rocks from northern Chile (18-22 S): implications for magmatism and tectonic evolution of the central Andes. Revista geológica de Chile, 27(2), 205-240.

Whittaker, A. C., Cowie, P. A., Attal, M., Tucker, G. E., & Roberts, G. P. (2007). Bedrock channel adjustment to tectonic forcing: Implications for predicting river incision rates. Geology, 35(2), 103-106.

Wörner, G., Uhlig, D., Kohler, I., & Seyfried, H. (2002). Evolution of the West Andean Escarpment at 18°S (N. Chile) during the last 25 Ma: uplift, erosion and collapse through time. Tectonophysics, 345(1–4), 183-198.

Wotzlaw, J. F., Decou, A., von Eynatten, H., Wörner, G., & Frei, D. (2011). Jurassic to Palaeogene tectono-magmatic evolution of northern Chile and adjacent Bolivia from detrital zircon U-Pb geochronology and heavy mineral provenance. Terra Nova, 23(6), 399-406.

10. Figures

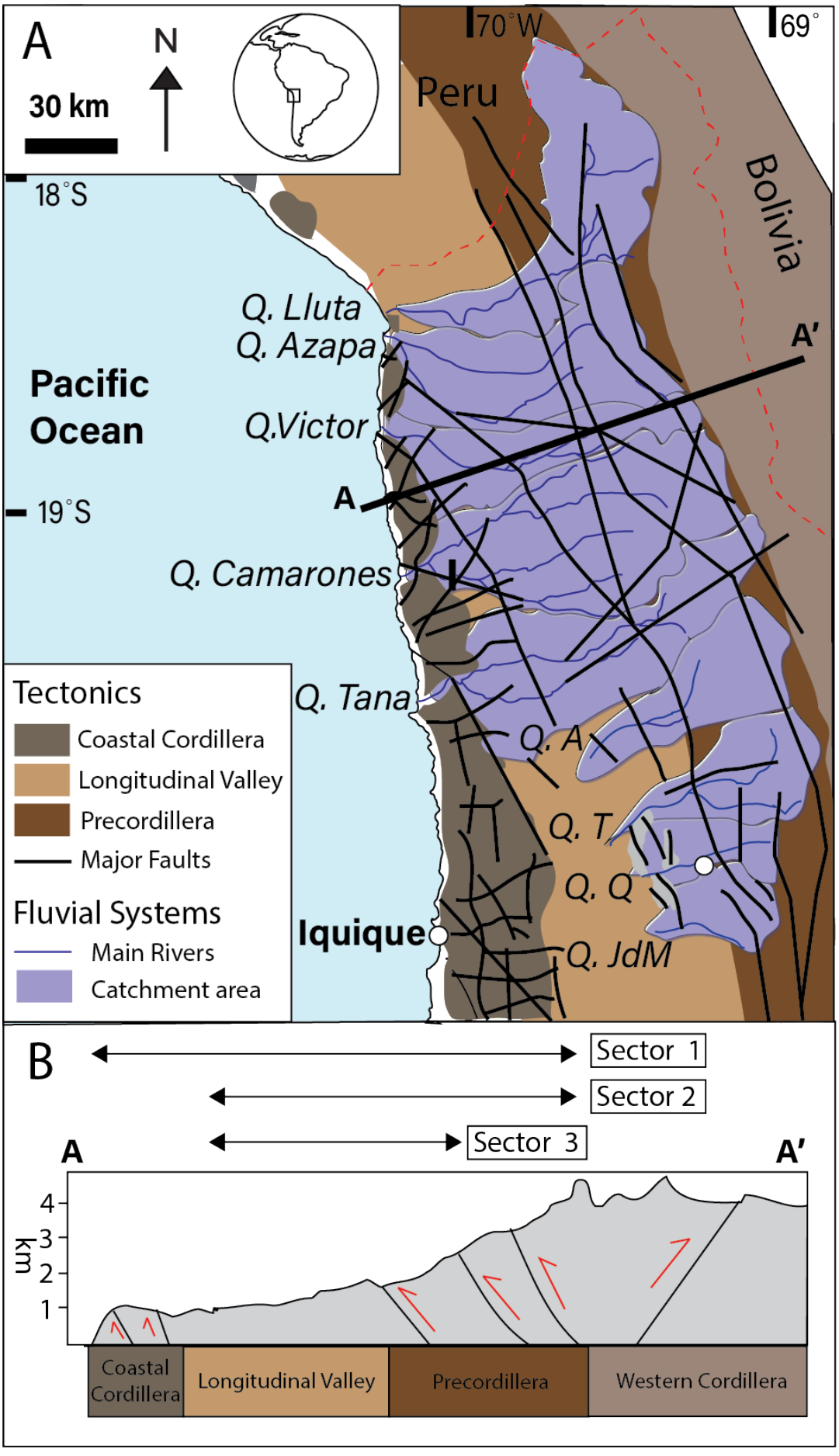
A
N
30 km
70°W
69°
Peru
Bolivia
18°S
Q. Lluta
Q. Azapa
Pacific
Ocean
Q.Victor
A'
A
19°S
Q. Camarones
Q. Tana
Q. A
Q. T
Q. Q
Iquique
Q. JdM
Tectonics
Coastal Cordillera
Longitudinal Valley
Precordillera
Major Faults
Fluvial Systems
Main Rivers
Catchment area
B
Sector 1
Sector 2
Sector 3
A
A'
km
4
3
2
1
Coastal Cordillera
Longitudinal Valley
Precordillera
Western Cordillera

Figure 1; a) Sketch of Central Andes showing the five morphotectonic provinces. The main sectors and the fluvial systems within them are highlighted showing catchment area (b) Cross section of main morphotectonic provinces, location shown in Figure 1A. Major tectonics features of the region (Garcia et al., 2004; Victor et al., 2004; Farías et al., 2005; Juez-Larre et al., 2010; Allmendinger and Gonzalez 2014;). Length of reach of the major Sectors (1-3) over the morphotectonic provinces are highlighted.

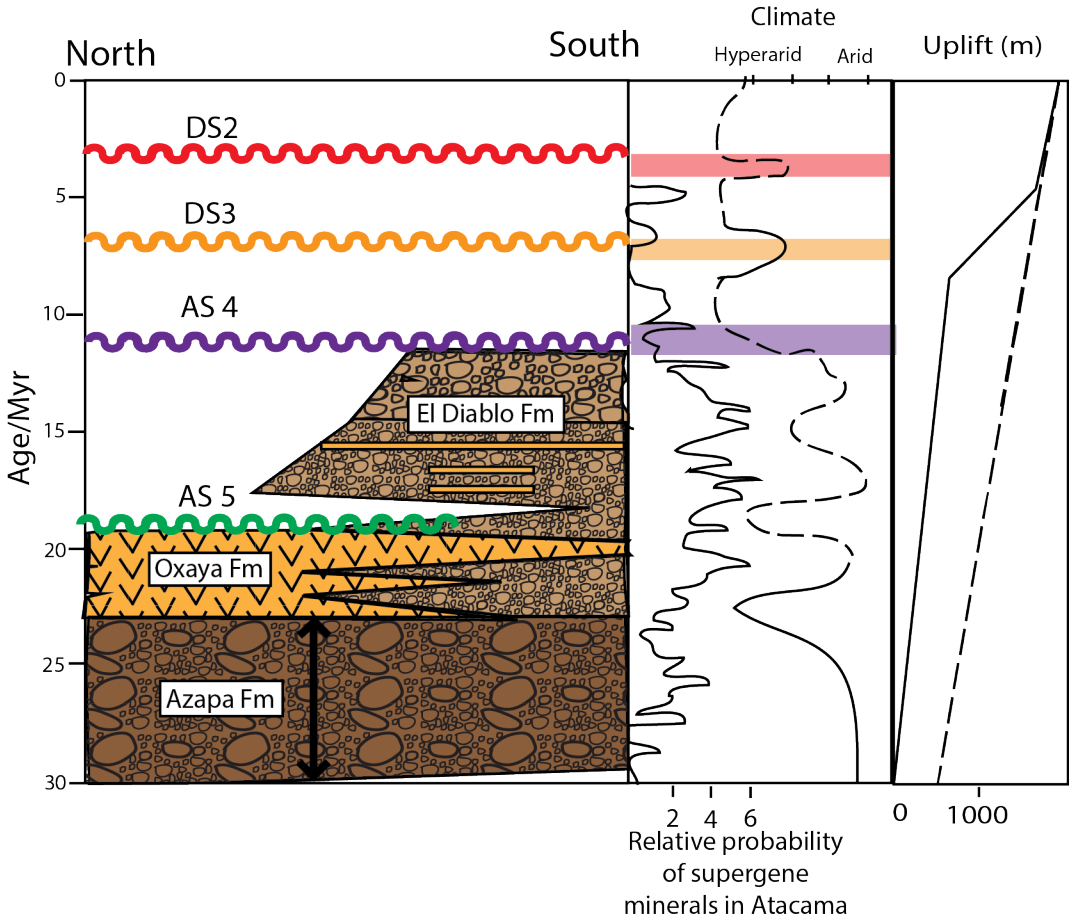

Figure 2; (from left to right) Basic sedimentary overview of the Longitudinal Valley in the study area with the main geomorphic surfaces (AS5, AS4, DS3 and DS2). Climate profile for Longitudinal Valley (Jordan et al. 2014 and Evenstar et al. 2017) with timing for main geomorphic surfaces highlighted and timing of supergene minerals in Atacama (Aranciabia et al. 2009). Elevation profiles for Longitudinal Valley from Evenstar et al. 2015. Solid line represents Late Miocene uplift and dashed line Early Miocene uplift.

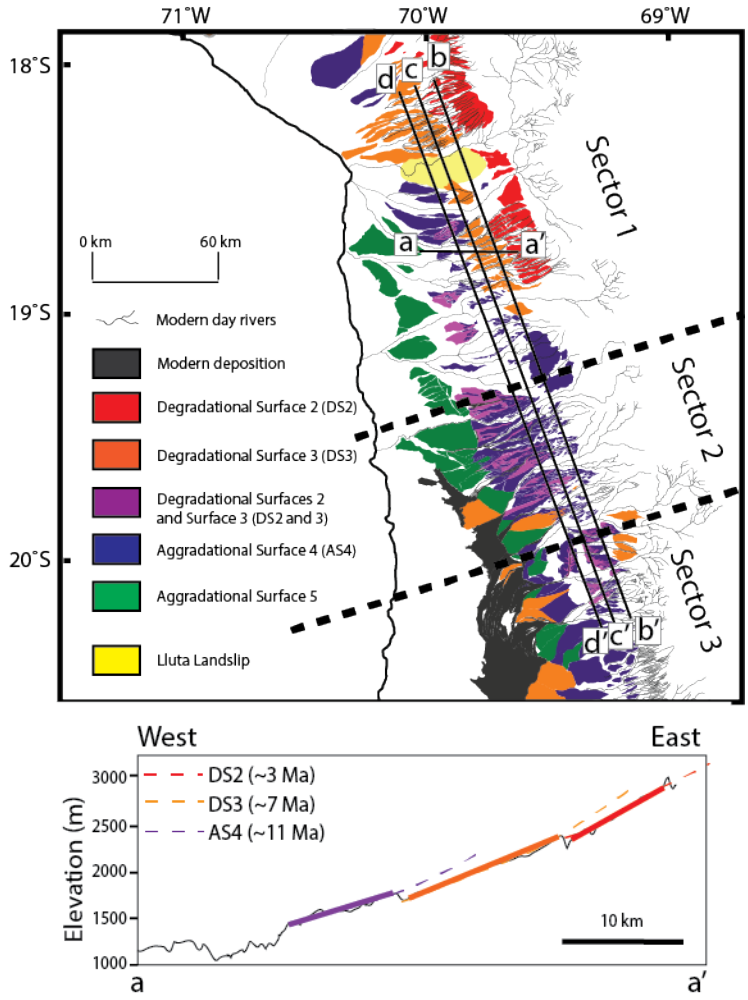

881

882 **Figure 3.** (Upper) Large scale map of Northern Chile showing the geomorphic
883 surfaces (1-5) that form the Pacific Paleosurface (PPS). Black lines highlight the
884 topographic cross sections (a-d) in figures 5. Black dashed lines separate regions of
885 Sector 1-3. (Lower) Profile A shows a profile taken west to east across the
886 Longitudinal Valley showing increasing incision of the paleosurfaces to the east
887 through time.

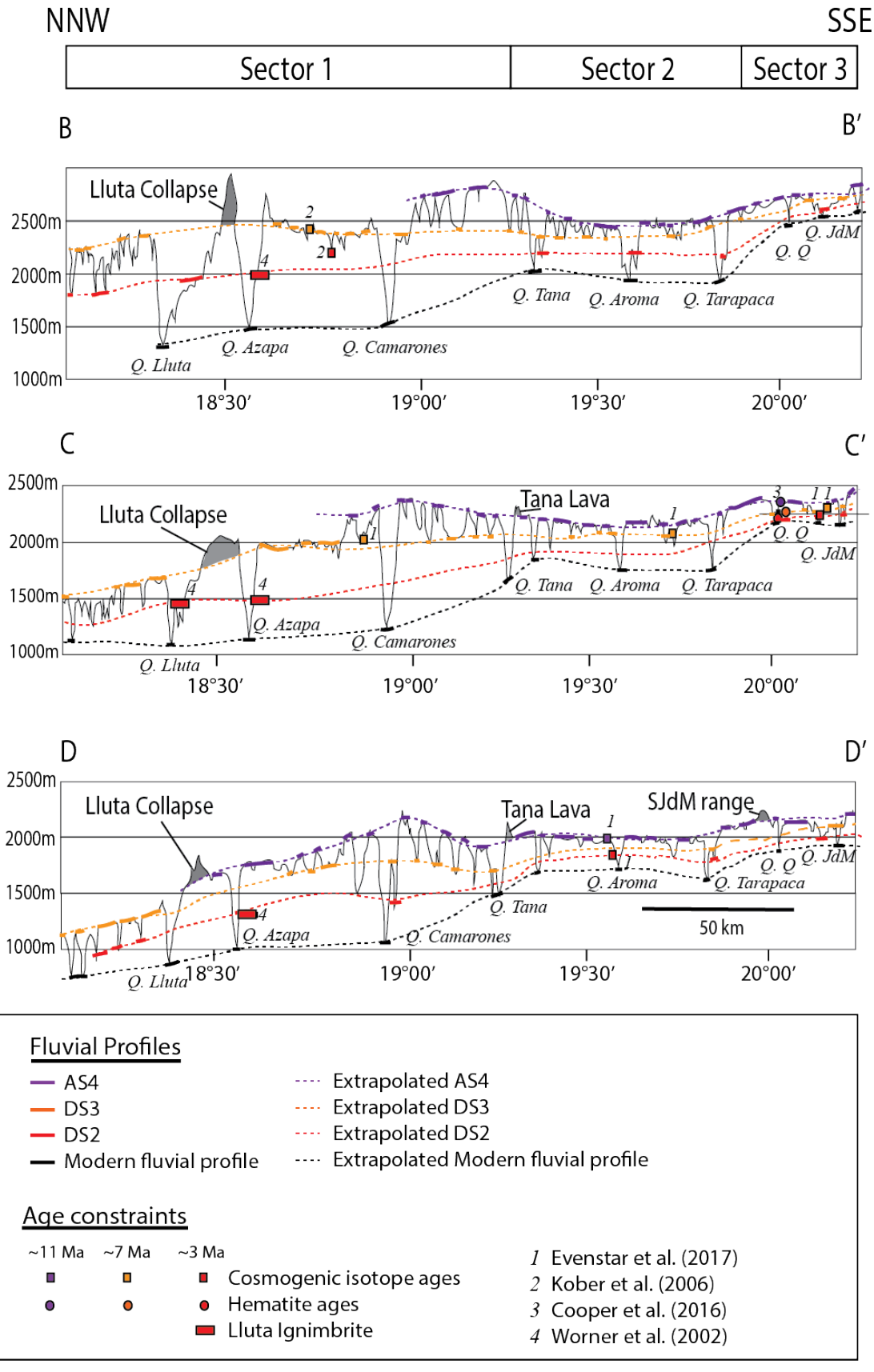

888

889 **Figure 4;** Three cross sections across the region. Locations shown in figure 3.

890 Profiles b-d are taken NNW to SSE. Black lines shows the topographic cross

891 sections across the region. Solid colour lines show the preserved parts of the surface

with the coloured dashed lines highlight the reconstructed paleo fluvial profiles associated with each surface (AS 4, DS3, DS2 and the modern). Grey areas represent anomalies on the topography profile. Key shows the main features that control the age of the surfaces.

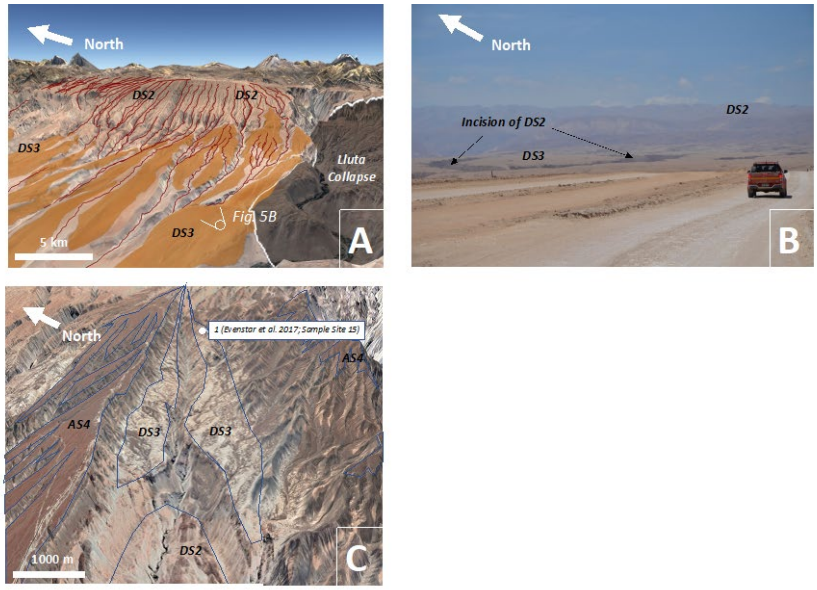

Figure 5; A) Google Earth image with 3x vertical exaggeration of DS2 cutting into DS3, leaving DS3 as a series of relict inselberg highs north of Quebrada Lluta. Location of photo of Figure 5B shown, B) Photo of same view taken from the field showing incision of DS3 by DS2 C) Google Earth image with 3x vertical exaggeration of DS3 and DS2 cutting into AS4 forming a lower terrace in Quebrada Camarones with site location of *insitu* exposure age dating in Evenstar et al. 2017.

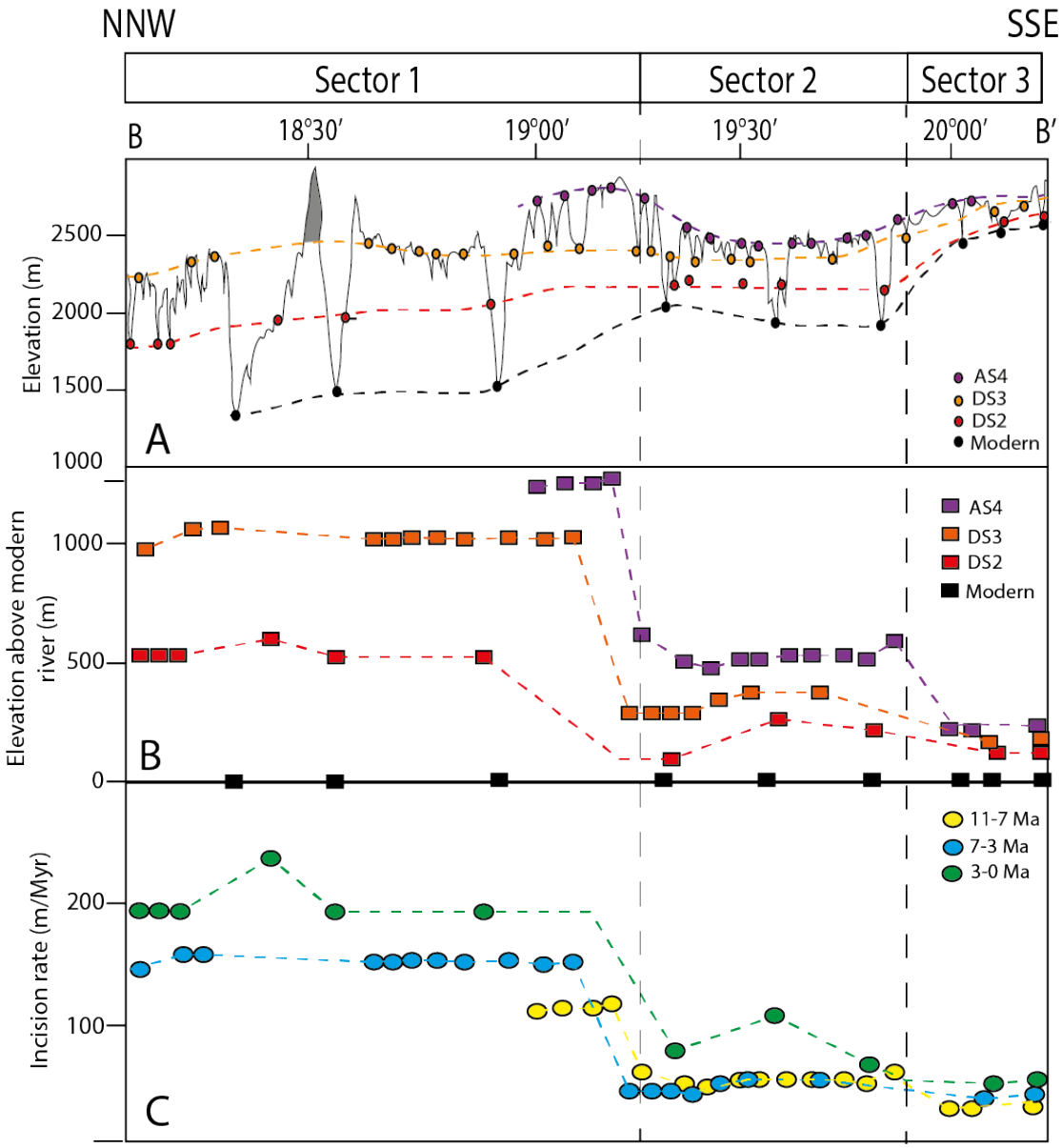

Figure 6; A- Cross section B showing the different paleo fluvial surfaces draped over an elevation profile. Coloured dots represent locations where the elevation was takes for Figure 6 B-C. **B** Shows the difference between paleo fluvial surfaces and modern fluvial profiles. **C** Incision rate through time calculated using the difference in elevation between the paleo fluvial surfaces and modern fluvial system divided by age of paleo fluvial surface.

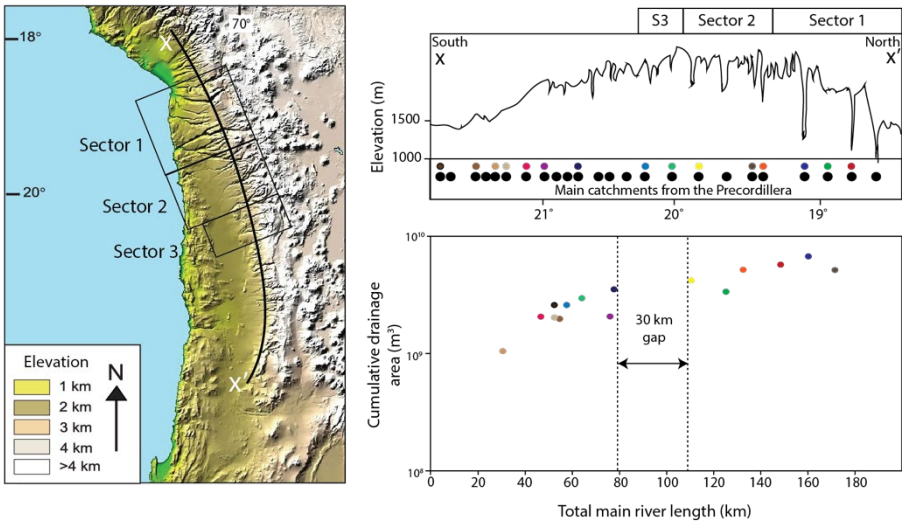

Figure 7; (Top) Elevation profile along the eastern edge of the Longitudinal Valley from Evenstar et al., 2017 highlighting study area (Sector 1, Sector 2 and Sector 3 (S3)). At the base of the elevation profile the black dots show the main fluvial systems from the Precordillera (the coloured dots relate to the dots in the cumulative drainage area graph below). (Bottom) cumulative drainage area of studied fluvial systems against length of fluvial system, this data was initially presented in Hoke et al. 2007 (supplementary material). a summary of cumulative drainage areas and fluvial length (distance from mouth) (Supplementary material in Hoke et al. 2007 which have been combined and summarized in this paper)